Environmental Science Advances

ROYAL SOCIETY OF CHEMISTRY

PAPER

View Article Online
View Journal | View Issue



Cite this: *Environ. Sci.: Adv.*, 2026, **5**, 1081

# Chronic PFOA and PFOS exposure triggers cellular oxidative stress and alters lipid levels as revealed through multi-omics analysis

Jenise Z. Paddayuman, †[a] Judith R. Cristobal, †[ab] Luane J. B. Landau, [c] Ashleigh L. Gagnon,[a] Omer Gokcumen, [c] Diana S. Aga *[ab] and G. Ekin Atilla-Gokcumen *[a]

Per- and polyfluoroalkyl substances (PFAS), or "forever chemicals," are linked to metabolic, immune, and neurotoxic disorders, yet their long-term cellular effects remain unclear. Using a 24 week chronic exposure model with non-transformed human epithelial cells, we examined responses to low, environmentally relevant concentrations of perfluorooctanoic acid (PFOA) and perfluorooctane sulfonic acid (PFOS). Integrated transcriptomic and lipidomic analyses revealed that despite minimal cellular accumulation, molecular changes emerged around week 17, marked by transcriptional signatures indicative of oxidative stress responses, cell survival pathways, and lipid metabolism. Our data suggests a multi-faceted model in which long-term PFOA and PFOS exposure induces oxidative stress mediated by SESN2 and SOD3, increases lipid biosynthesis *via* SREBP pathway, and causes compound-specific disruptions of membrane lipids. These findings highlight the importance of multi-omic, time-resolved approaches in uncovering the mechanisms of chronic low-dose chemical exposure and provide a foundation for future *in vivo* studies.

Received 9th October 2025
Accepted 20th February 2026

DOI: 10.1039/d5va00353a

rsc.li/esadvances



### Environmental significance

Perfluorooctanoic acid (PFOA) and perfluorooctane sulfonic acid (PFOS) are persistent pollutants linked to various adverse health effects. Many research studies focus on high doses, which overlooks the risks associated with real-world low-level exposure. This study aimed to address this gap by exposing human epithelial cells to environmentally relevant concentrations of PFOA and PFOS (10 nM) over a six-month period. Our findings indicate that chronic, low-dose exposure to PFOA and PFOS results in cumulative disruptions to lipid profiles and persistent cellular stress responses. These insights provide a solid framework for future *in vivo* studies examining the relationship between genetic and lipid alterations and PFAS-induced toxicity.

## 1. Introduction

Perfluorooctanoic acid (PFOA) and perfluorooctane sulfonic acid (PFOS) are legacy per- and polyfluoroalkyl substances (PFAS) that are no longer manufactured or used in several countries, yet they persist in the environment[1,2] due to their stability.[3] Their remarkable resistance to degradation[4] has led to the bioaccumulation of PFOA and PFOS in ecosystems over decades, resulting in long-term contamination at detectable levels in wildlife and human populations. This persistence has earned PFAS the nickname "forever chemicals".[4]

PFOA and PFOS have been detected in various human tissues, indicating their high potential for bioaccumulation.[5] Exposure to these chemicals has been associated with metabolic disorders,[6,7] immune dysregulation,[8,9] and neurotoxicity.[10–12] Despite being phased out globally due to health concerns, their impacts continue to affect the environment and humans to this day. However, the molecular mechanisms driving PFAS toxicity remain poorly understood. At the molecular level, PFAS can interact with lipids,[13,14] proteins,[15] and nucleic acids[16] as evidenced in biochemical studies. Their amphiphilic structure enables them to interact with lipid membranes, potentially affecting membrane fluidity and permeability.[17,18] They can also bind proteins with hydrophobic domains, such as serum albumin,[19] peroxisome proliferator-activated receptors (PPARs),[16] and fatty acid-binding proteins,[20] potentially interfering with key regulatory functions. Despite these known interactions, the specific cellular

[a]*Department of Chemistry, University at Buffalo, The State University of New York (SUNY), Buffalo, New York 14260, USA. E-mail: dianaaga@buffalo.edu; ekinatil@buffalo.edu; Tel: +1 (716) 645-4220; +1 (716) 645-4130*

[b]*Research and Education in eNergy, Environment and Water (RENEW) Institute, University at Buffalo, The State University of New York (SUNY), Buffalo, New York 14260, USA*

[c]*Department of Biological Sciences, University at Buffalo, The State University of New York (SUNY), Buffalo, New York 14260, USA*

† These authors contributed equally to this work.

pathways and biological processes disrupted by PFAS remain unclear.

One of the major challenges in understanding the biological pathways affected by PFAS in living systems stems from the discrepancy between laboratory exposure models and real-world environmental exposure. Most experimental studies, including *in vitro* models, employ short-term exposures at relatively high concentrations of PFAS (5–125 μg $mL^{-1}$),[21] specifically 10–250 μM concentration range for PFOA and PFOS. Meanwhile, concentrations at contaminated sites do not exceed ~150–200 nM for PFOA and PFOS[2] and concentrations of PFOA and PFOS in human serum are typically even lower, ranging from ~2.8–10.4 nM and ~9.0–104.2 nM, respectively.[22,23] As a result, existing models may fail to capture the cumulative or adaptive biological responses that emerge only with prolonged, low-level exposure, limiting the translational relevance of these findings to real-world conditions.

In this study, we employed integrated transcriptomic and lipidomic analyses to investigate the cellular effects of long-term, chronic PFOA and PFOS exposure. This approach, which has not been extensively utilized in the study of PFAS *in vitro,* allows for a comprehensive understanding of the molecular alterations induced by these compounds. To better reflect real-world exposure, we conducted a time-course experiment using human retinal pigment epithelial cells (hTERT RPE-1), exposing them to environmentally relevant concentrations of PFOA or PFOS over a six-month period. This cell line has been characterized for genomic and transcriptomic stability over time, confirming stability across batches and passage numbers.[24,25] Using RNA sequencing and high-resolution mass spectrometry-based targeted lipidomics, we profiled molecular responses to realistic PFAS exposure across time.

Our findings offer new insights into the systems-level response to prolonged, low-concentration PFAS exposure. We found that rather than a single dominant pathway, PFOA and PFOS toxicity arise from cumulative and multifactorial disruptions in key cellular processes, including dynamic remodeling of the lipidome and sustained activation of oxidative and cellular stress responses. Together, our results provide specific mechanistic hypotheses and a robust framework for future *in vivo* studies aimed at linking genetic and lipid-level responses to PFAS-induced toxicity.

# 2. Materials and methods

## 2.1. Chemicals and other reagents

hTERT RPE-1 cells were purchased from the American Type Culture Collection (Manassas, VA). Dulbecco's modified Eagle media (DMEM)/Ham's F-12 (50 : 50), fetal bovine serum (FBS), trypsin, and penicillin/streptomycin (p/s) antibiotic cocktail were purchased from Corning (Corning, NY). Micro bicinchoninic acid (BCA) assay kit was purchased from G Biosciences (St. Louis, MO).

PFOA (95% purity) and PFOS (98% purity) were purchased from Millipore Sigma (Burlington, MA). $^{13}C$-labelled standards, including M8PFOA, M8PFOS, M4PFOA, and M4PFOS, were purchased from Wellington Laboratories (Guelph, ON). Ammonium acetate was purchased from J.T. Baker (Randnor Township, PA). Liquid chromatography-mass spectrometry (LC-MS) grade methanol (MeOH), isopropanol, and acetonitrile were purchased from Millipore Sigma (Burlington, MA). LC-MS grade chloroform was purchased from Honeywell Research Chemicals (Morris Plains, NJ). Type I water (18.2 MΩ cm) was generated using a Barnstead Nanopure Diamond (Waltham, MA) purification system. The LC-MS columns and guard columns used for PFAS analysis and lipidomics analysis were obtained from Restek Corporation (Bellefonte, PA) and Phenomenex (Torrance, CA), respectively. MassHunter™ Qualitative analysis, which was utilized for data analysis, was obtained from Agilent Technologies (Santa Clara, CA).

## 2.2. Cell culture, PFAS exposure, and cell collection

The culturing, PFAS exposure, and subsequent collection of hTERT RPE-1 cells were conducted following a recently published protocol.[13] Briefly, hTERT RPE-1 cells were cultured in DMEM/F-12 (50 : 50) with L-glutamine and 15 mM HEPES. The media was supplemented with 10% (v/v) FBS and 1% (v/v) p/s. Cells were grown at 37 °C and 5% $CO_2$ until they reached 80–90% confluency for use. Cells were treated with 0.01% MeOH (vehicle control), 10 nM PFOA or 10 nM PFOS in 0.01% MeOH in separate 10 cm polystyrene-treated culture dishes and cultured by passaging twice a week (*i.e.* every 3–4 days) for 24 weeks ($n = 3$). At designated time points (24 hours, 7 weeks, 17 weeks, and 24 weeks), cells treated with MeOH, PFOA, and PFOS at 80–90% confluency were collected. Cells were washed with cold 1× phosphate-buffered saline (PBS) and collected by centrifugation at 300 relative centrifugal force (rcf) for 5 min at 4 °C. The media was decanted, and the cells were washed two more times with cold 1× PBS to remove residual media using the centrifugation protocol previously described. The cell pellet was resuspended in 500 μL of cold 1× PBS. For PFAS uptake analysis, 50 μL aliquots were set aside for protein quantification through the BCA assay. Afterward, the cell pellets were collected by centrifugation and stored at −80 °C for subsequent analysis: bioaccumulation, lipidomics, and transcriptomics. At every exposure time point, each treatment group included at least triplicate samples ($n = 3$) for each analysis.

## 2.3. PFOA and PFOS extraction and liquid chromatography-tandem mass spectrometry (LC-MS/MS) data acquisition for cellular uptake

The PFAS-treated cells were extracted following a published protocol.[10] Cell pellets at various time points that were treated individually with PFOA and PFOS, along with their corresponding MeOH as vehicle control, were resuspended in 1 mL of cold MeOH spiked to contain corresponding 90 ppb mass-labelled PFAS standards (M8PFOA and M8PFOS) as surrogates. The cell suspension was sonicated using Fisherbrand Model 120 Sonic Dismembrator probe sonicator, set at 40% power with 30 second pulses and 30 second rests while on a cold metal block. After sonication, samples were centrifuged at 16 900 rcf for 12 min at 4 °C. Carefully, 900 μL of the resulting supernatant was transferred into a 4 mL dram vial. The

 

remaining pellets were subjected to a second extraction by adding 1 mL of cold MeOH and repeating the sonication and centrifugation steps. The supernatants from both extractions were combined and evaporated to dryness using a nitrogen evaporator. Final extracts were reconstituted with the mobile phase system of 50 : 50 (A) 5 mM ammonium acetate in water with 5% acetonitrile, pH 3.8; and (B) 50 : 50 MeOH : acetonitrile (v/v) spiked with 50 ppb of internal standards, M4PFOS and M4PFOA.

PFOA and PFOS samples, along with their corresponding MeOH controls, were analyzed following a published method[26] *via* liquid chromatography-tandem mass spectrometry (LC-MS/MS) using a Thermo TSQ Quantum Ultra™ triple quadrupole mass spectrometer and Agilent 1200 liquid chromatography. Separation of each 10 μL injection was achieved using a Raptor C18 analytical column (100 mm, 2.7 μm), equipped with a 5 mm guard column containing identical stationary phase material, using an elution gradient and 0.37 mL $min^{-1}$ flow rate. The gradient profile consisted of 50% (B), ramped to 95% (B) over 8 min and was held for 3 min before returning to the starting mobile phase of 50% (B). The total run time for each injection was 18 min. The mass spectrometer was operated in negative mode as $[M - H]^-$ using an electrospray ionization voltage of −3000 V and capillary temperature of 220 °C. Selected reaction monitoring mode were employed, and two transitions (Table S1) were monitored for each analyte to ensure specificity.

### 2.4. Limit of quantification (LOQ) and limit of detection (LOD) determination for PFOS and PFOA

Ten-10 cm plates of confluent hTERT RPE-1 cells were collected, protein quantified, and extracted following the above protocol. To create the matrix-matched calibration curves, for each PFOA and PFOS, seven-point calibration with replicates ($n = 3$) were prepared using serial dilution starting with 1 ppb to 64 ppb in a diluent matrix containing 50 ppb each of M8PFOA and M8PFOS as internal standards for normalization. The slope ($S$) was then obtained from the calibration curves (Fig. S1). For the lowest concentration (1 ppb), seven replicates were made to get the standard deviation of the response (Sy). Prepared solutions were analyzed using LC-MS/MS as described above. Finally, the limit of detections (LODs) and limit of quantifications (LOQs) were calculated using the formula LOD = 3(Sy/$S$) and LOQ = 10(Sy/$S$) (Table S2).

### 2.5. RNA extraction, library preparation, sequencing, and analysis

Frozen cell pellets treated individually with PFOA and PFOS for 24 hours, 7 weeks, 17 weeks, and 24 weeks ($n = 3$) that were previously stored at −80 °C were transported on dry ice to Azenta Life Sciences (South Plainfield, NJ) for RNA extraction and RNA-seq analysis. Azenta's RNA-seq workflow comprises five steps, including experimental design, extraction, library preparation, sequencing, and data analysis. RNA from cells was extracted, and RNA molecules of interest were purified to ensure high quality and sufficient quantity prior to proceeding with analysis. After which, single-stranded RNA was converted to double-stranded complementary DNA (cDNA) strands in a reverse transcription reaction. Sequencing adapters and barcodes were then added to create RNA-seq libraries which were subsequently analyzed with Next Generation Sequencing (NGS) using Illumina NovaSeq™6000 or Illumina Hiseq®X. The data were then evaluated, and biologically relevant information was extracted. Briefly, sequencing reads were pre-processed and trimmed to remove adapter sequences and low-quality bases. Trimmed reads were then mapped to the reference genome, followed by expression quantification and transcripts per million (TPM) calculation. Differential expression analysis was performed using DESeq2,[27] comparing treatments to the control: PFOA *vs.* MeOH, PFOS *vs.* MeOH, and PFOA *vs.* PFOS. Note that MeOH 24H was used as a control for all time point comparisons involving both PFOA and PFOS. Gene Ontology (GO) enrichment analysis was conducted for significant genes ($|\log_2$fold change$| > 1$ & adjusted $p < 0.05$) in each comparison using gProfiler.[28] To investigate shared gene expression patterns between PFOA and PFOS at 24 weeks, we identified differentially expressed genes (DEGs) common to both PFOA *vs.* MeOH and PFOS *vs.* MeOH comparisons at 24 weeks and performed GO enrichment analysis on this shared gene set. We also conducted an analysis of highly differentially expressed genes specific to PFOA and PFOS at 24 weeks.

### 2.6. Lipid extraction and liquid chromatography-mass spectrometry (LC-MS) data acquisition for lipidomics analysis

Lipid extraction, sample preparation, and analysis were carried out as described in a published protocol.[29,30] Cell pellets were resuspended in 550 μL of cold 1× PBS, and 50 μL of aliquots were set aside for protein quantification. An additional 500 μL of cold 1× PBS was added, and the cell pellets were transferred to a 7 mL Dounce homogenizer. To the suspension, 1 mL of cold MeOH and 2 mL of cold chloroform were added, and the mixture was homogenized with 30 strokes. The homogenized solution was transferred to a 4 mL dram vial and centrifuged at 500 rcf for 10 min at 4 °C. The chloroform layer, containing the lipids, was carefully extracted and transferred to a new dram vial. This layer was evaporated to dryness using a nitrogen evaporator and subsequently stored at −80 °C until further analysis by LC-MS.

Lipid extracts were spiked with C17:0 Ceramide (C17-Cer), C17 Sphingomyelin, $d^9$-oleic acid, C17 Glucosyl(b) Ceramide (C17 GluCer), C39:0 triacylglycerol (C39-TAG), C18-$d^7$-sphingosine as internal standards and reconstituted with chloroform. Analysis was carried out in negative and positive modes *via* an Agilent 1260 HPLC system in tandem with an Agilent 6530 Jet Stream ESI-QToF-MS system. Separation of each 15 μL injection was achieved using a Gemini C18 column (5 μm, 4.6 mm × 50 mm) for negative mode, while a Luna C5 column (5 μm, 4.6 mm × 50 mm) was used for positive mode. The mobile phase system consisted of: (A) 95 : 5 water : MeOH and (B) 60 : 35 : 5 isopropanol : MeOH : water for both modes, with the addition of ammonium hydroxide for negative mode, and formic acid and ammonium formate for positive mode. The gradient profile consisted of 0% (B) ramped to 100% (B) over 65 min and was

held for 7 min before returning to the starting mobile phase of 0% (B). The total run time for each injection was 80 min. The mass spectrometer was operated using a DualJSI fitted electrospray ionization source with voltage of 3500 V. The drying gas temperature was set to 350 °C with a flow rate of 12 L $min^{-1}$. Lipid species were targeted by extracting the corresponding *m*/*z* (Table S3) for each ion in MassHunter™ Qualitative Analysis software (v11). Peak areas for each ion were integrated and represented as abundance. Relative abundances used in heatmaps for the PFAS treatments ($n = 3$) were normalized to the individual MeOH control.

### 2.7. Statistical analysis

All statistical analyses were performed using GraphPad Prism (v10.4.2) or R software (v4.2.2). The data presented are the averages of three independent replicates. For PFAS bioaccumulation studies, *p*-values were calculated using an unpaired *t*-test. Lipidomics analysis used a paired two-tailed *t*-test with directly matched sample and vehicle control within the same biological replicate, with $p < 0.05$ considered significant. In GO enrichment analysis for transcriptomics, $|\log_2 \text{fold change}| > 1$ & adjusted *p*-value < 0.05 were set as the threshold for significant genes in gProfiler.

## 3. Results and discussion

### 3.1. A novel *in vitro* model of prolonged PFAS exposure reveals limited cellular accumulation

To investigate the cellular effects of PFAS at concentrations reflecting realistic environmental exposure, we exposed hTERT RPE-1 cell line to either 10 nM of PFOA (4.14 μg $L^{-1}$) or 10 nM PFOS (5.00 μg $L^{-1}$), individually, over 24 weeks (Fig. 1A). This experimental design provides a suitable framework for modeling the long-term cellular impact of exposure. First, the exposure levels fall within the range detected in contaminated groundwater sources,[2] and human blood serum.[22,23] Second, hTERT RPE-1 cells are a non-cancerous model that more accurately recapitulate normal cellular homeostasis than commonly used transformed, cancer-derived cell lines[13] and have often been used to investigate the normal physiological roles of human genes.[31] Studies have also confirmed the genomic and transcriptomic stability of hTERT RPE-1 cells over time,[24,25] making this system ideal for chronic exposure. Over the 24 week period, vehicle control-treated cells and PFOA/PFOS-treated cells consistently displayed stable cell morphology and growth characteristics, indicated by passage numbers. Thus, hTERT RPE-1 is robust to effects of senescence and passage-based biases over a 24 week period.

To assess the cellular accumulation of PFAS, we quantified intracellular levels of PFOA and PFOS at 24 hours, 7 weeks, 17 weeks, and 24 weeks (Methods, Tables S2 and S4). We selected 24 hours to capture acute, short-term exposure and 24 weeks to model chronic, long-term accumulation.[32] While human exposure to PFAS is lifelong, we used the 24 weeks *in vitro* exposure as it was feasible to do in the laboratory setting. The intermediate time points at 7 weeks and 17 weeks were selected arbitrarily to provide resolution of temporal trends and to capture potential nonlinear or progressive changes in PFAS accumulation that might not be evident from short- and long-term endpoints alone. Surprisingly, we observed no significant accumulation of PFOS over time (Fig. 1B and Table S4). Specifically, PFOS exhibited an initial uptake within the first 24 hours, reaching a mean concentration of 0.40 ng $mg^{-1}$ of protein, followed by a slight decline at 17 weeks and stabilization at 24 weeks (Table S4). In contrast, we were unable to detect PFOA, as its concentrations at the cellular level were below the limit of detection of our method (LOD = 0.75 ng PFOA per mg protein, Fig. S1 and Tables S2, S4). The observation that PFOS does not accumulate in cells over time suggests that organismal-level bioaccumulation of PFOS may depend on mechanisms beyond direct intracellular uptake, such as accumulation in extracellular components or the presence of multiple cell types that may accumulate PFOS *via* different mechanisms within complex tissue environments.

### 3.2. Comparative gene expression profiles reveal time-dependent, system-level responses to prolonged PFAS exposure

Our findings of minimal or undetectable intracellular bioaccumulation prompted us to investigate whether low-level exposure could still elicit a biological response over time. To address this, we performed comparative transcriptomic analyses across multiple time points under prolonged PFAS exposure (Fig. 1C and Table S5). Using a conservative threshold (adjusted *p*-value < 0.05, $|\log_2 \text{fold change}| > 1$; see Methods), we observed virtually no differentially expressed genes at the 24 hour and 7 week time points for either PFOA or PFOS. However, at 17 weeks, we detected a significant increase in transcriptional activity, with 442 and 356 differentially expressed genes for PFOA and PFOS, respectively, compared to MeOH-treated controls (Fig. 1D and Table S5). Thus, the transcriptomic response starts between 7- and 17 week time points, intensifying further with 1415 and 1368 genes being differentially expressed at 24 weeks for PFOA and PFOS, respectively. We note that the genes involved in cell cycle arrest, including CDKN1A, CDKN2A, and TP53, were not significantly upregulated across the four treatment time points, supporting both the transcriptomic stability of the hTERT-RPE-1 cell line and the absence of cell cycle arrest. Overall, our results suggest that even in the absence of significant intracellular accumulation, prolonged low-level PFAS exposure induces a delayed but robust transcriptomic response, affecting hundreds to thousands of genes over time.

### 3.3. Cellular stress is the major driver of convergent transcriptional responses to PFAS exposure

We observed a similar total number of differentially expressed genes in response to both PFOA and PFOS treatments over 24 weeks. To determine whether these transcriptional changes reflected a shared molecular response, we compared the magnitude and trends in the changes in gene expression upon PFOA and PFOS exposure (Table S5). This analysis is critical, as PFOA and PFOS, although structurally related, differ in key

 

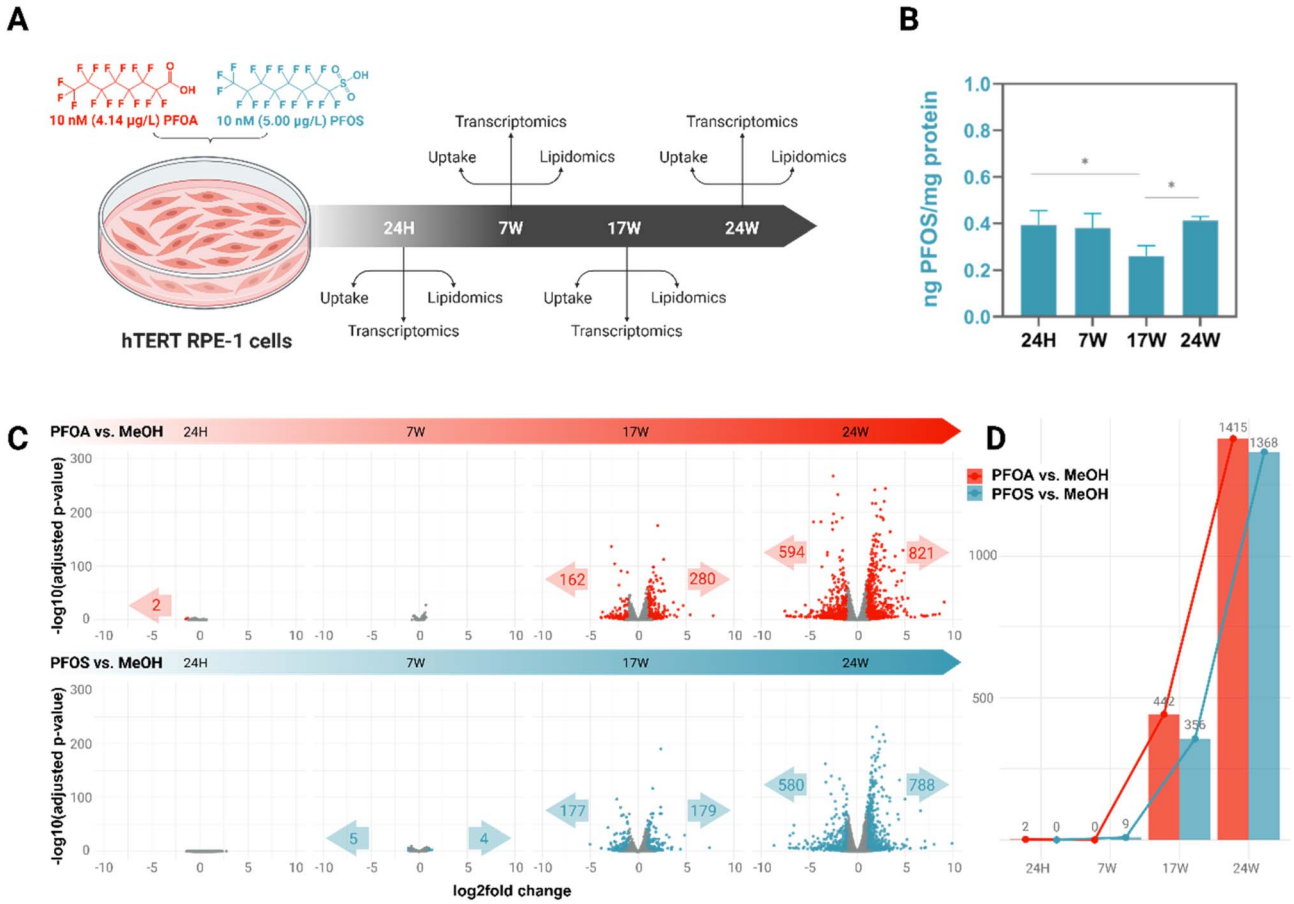


Fig. 1 *In vitro* model of chronic PFAS exposure and overview of gene expression changes in hTERT RPE-1 cells. (A) Experimental design investigating the uptake, lipidomic, and transcriptomic alterations in hTERT retinal pigment epithelial (hTERT RPE-1) cells exposed to PFOA (red) and PFOS (blue) over 24 weeks. (B) PFOS uptake in hTERT RPE-1 cells. Data are represented as the mean of three independent replicates. *p*-values were calculated using an unpaired *t*-test, with $p < 0.05$ considered as significant. (C) Volcano plots showing differentially upregulated (right arrow) and downregulated (left arrow) genes with prolonged exposure to PFOA and PFOS. Colored dots indicate adjusted $p < 0.05$ and $|\log_2 FC| > 1$. (D) Total differentially regulated genes observed over 24 weeks.

biological properties, including half-life,[5] tissue accumulation, and interaction with host biomolecules.[33] For example, PFOS exhibits a longer half-life, accumulates more readily in tissues, and binds more strongly to proteins, with well-established effects on lipid homeostasis in liver cells.[5,34]

Despite these differences, we found a strong positive correlation in gene expression fold changes between PFOA and PFOS treatments compared to vehicle-treated control cells (Pearson's $r = 0.788$; Fig. 2A). This high correlation suggests a core transcriptional response to PFOA and PFOS exposure that is largely independent of the specific chemical characteristics of individual compounds.

To understand the biological processes underlying this response, we performed Gene Ontology (GO) enrichment analyses (see Methods, Table S6). The enriched categories shared between PFOA- and PFOS-responsive genes included several biological processes broadly associated with external stress, including oxidative stress, lipid metabolism, and cell death (Fig. 2B). To further dissect the pathways involved in chronic cellular response to PFAS exposure, we conducted a targeted literature review of genes[35–40] (Fig. 2C) contributing to these enriched categories. This analysis yielded a shortlist of five key genes involved in oxidative stress response and the regulation of lipid metabolism: Superoxide dismutase 3 (SOD3), Sestrin 2 (SESN2), stearoyl-CoA desaturase (SCD), acyl-CoA synthetase long-chain family member 5 (ACSL5), and Chac glutathione-specific gamma-glutamylcyclotransferase 1 (CHAC1). We discuss their regulation and potential relevance to exposure in the following section.

Among genes associated with oxidative stress listed in Fig. 2C, two stood out as central players: Superoxide dismutase 3 (SOD3) and Sestrin 2 (SESN2), both showing high correlation and consistent upregulation across the exposure period. SOD3 encodes an extracellular enzyme activated by oxidative stress that converts superoxide radicals, major inducers of cellular damage, into less reactive hydrogen peroxide.[41] SESN2, in contrast, functions intracellularly. It is also induced by oxidative stress and acts as a direct scavenger of reactive oxygen species (ROS), while also regulating broader intracellular stress responses to maintain homeostasis.[42]

The coordinated upregulation of SESN2 and SOD3 exemplifies a robust antioxidant defense response to prolonged PFAS

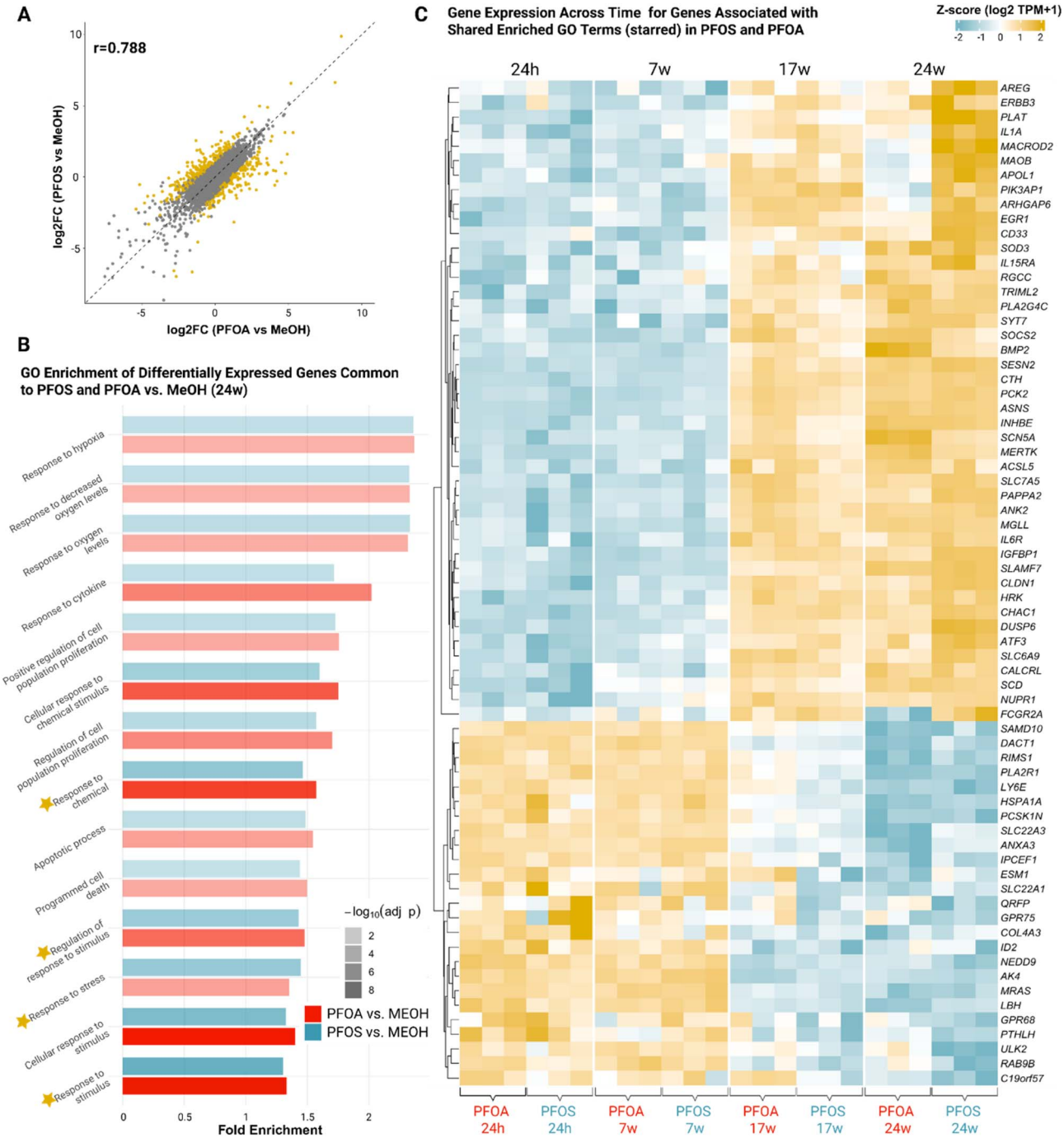


Fig. 2 Comparative analysis of gene expression highlighting the transcriptional responses to prolonged PFOA and PFOS exposure of hTERT RPE-1 cells. (A) Similarity and consistency in gene expression changes for PFOA and PFOS when compared to the control at 24 weeks. Yellow dots represent genes that are differentially expressed between PFOA and PFOS. (B) GO terms related to cellular response and chemical exposure identified from DEGs ($p < 0.05$ and $\log_2FC > 1$) in both comparisons (PFOA *vs.* MeOH and PFOS *vs.* MeOH) at 24 weeks. The *y*-axis shows selected GO terms, the *x*-axis indicates fold enrichment, and color transparency represents adjusted *p*-values. (C) Heat map showing expression trends across time of enriched genes related to the following GO terms: "response to stress", "response to stimulus", "regulation of response to stimulus", and "response to chemical". Genes shown were identified as differentially expressed at 24 weeks and displayed to depict temporal expression patterns.

exposure (Fig. 3 and Table S5). As we expand upon below, oxidative stress likely serves as a central axis that integrates multiple downstream effects of chronic PFAS exposure, including lipid biosynthesis and activation of cell death pathways.

We performed a parallel differential expression analysis comparing PFOA- and PFOS-treated cells at the 24 week time

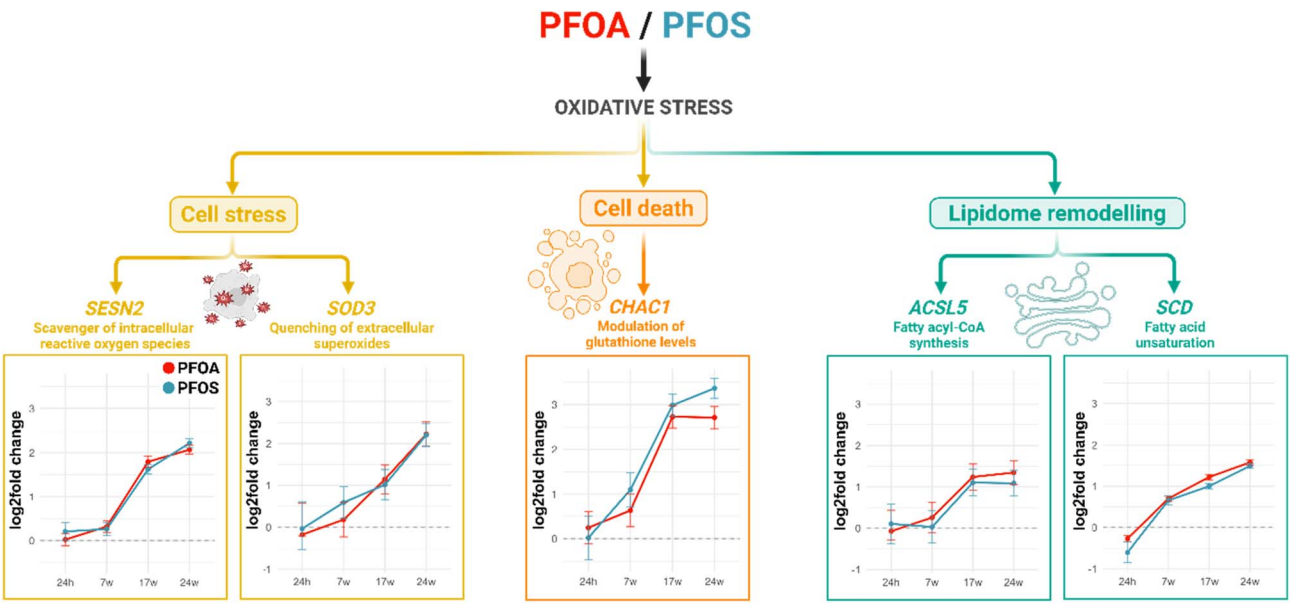


Fig. 3 Transcriptomic profiling reveals that chronic exposure to PFOA and PFOS elicits oxidative stress and cellular remodeling responses. Five shortlisted genes and their expression trends based on analysis in Fig. 2. Shown are upregulated expression levels ($log_2$fold change) of representative genes involved in oxidative stress [Sestrin 2 (SESN2), Superoxide dismutase 3 (SOD3)], cell death [ChaC glutathione-specific gamma-glutamyl cyclotransferase 1 (CHAC1)], and lipid metabolism [Acyl-CoA synthetase long-chain family member 5 (ACSL5), Stearoyl-CoA desaturase (SCD)]. Data are presented as $log_2$fold change ± SEM from three independent replicates.

point (Fig. S2 and Table S7). Gene ontology (GO) analysis of these differentially expressed genes revealed both shared and compound specific pathways perturbed by chronic PFAS exposure. Notably, PFOS highly enriched pathways related to inflammatory signaling, response to xenobiotic stimulus, and membrane-associated processes. However, without accompanying phenotypic evidence or functional assays, the biological implications of these PFOS specific pathway enrichments remain uncertain, and their mechanistic relevance requires further investigation.

### 3.4. Lipid and cell death-related gene expression is driven by PFAS-induced oxidative stress

We next investigated key genes involved in lipid biosynthesis among the enriched categories shared between PFOA- and PFOS-responsive genes (Fig. 2B, C and Table S5). Two enzymes stood out for their central roles in lipid metabolism: stearoyl-CoA desaturase (SCD) and acyl-CoA synthetase long-chain family member 5 (ACSL5). SCD1, which catalyzes the conversion of saturated fatty acids to monounsaturated fatty acids,[43,44] was among the most highly upregulated genes following PFAS exposure (Fig. 3 and Table S5). This observation is especially compelling in the context of oxidative stress. Prior studies have shown that oxidative stress is associated with the intracellular accumulation of unsaturated fatty acids, a condition that promotes cell death.[45] Thus, SCD-mediated desaturation may act as a protective mechanism to restore lipid homeostasis and reduce lipid-induced apoptotic signaling under oxidative stress conditions.

Similarly, ACSL5, which converts long-chain fatty acids (16–20 carbons) into their corresponding acyl-CoA derivatives,[46] was also upregulated. Long-chain fatty acid oxidation is a well-known source of ROS due to electron leakage during mitochondrial β-oxidation.[47] By converting free fatty acids into acyl-CoA forms, ACSL5 may help limit the availability of substrates for ROS-generating oxidation processes, thereby alleviating lipotoxic stress. Together, these changes suggest that shifts in lipid biosynthetic gene expression during chronic, low-level PFAS exposure represent a broader adaptive response to PFAS-induced oxidative stress.

Lastly, ChaC glutathione-specific gamma-glutamyl cyclotransferase 1 (CHAC1), a gene involved in glutathione metabolism and linked to oxidative cell death pathways, was among the genes that the enrichment analysis revealed (Fig. 2C). CHAC1 catalyzes the degradation of glutathione into 5-oxo-proline and a cysteinyl-glycine (Cys-Gly) dipeptide.[48,49] Similar to the lipid-related genes, CHAC1 was significantly upregulated in response to PFAS exposure (Fig. 2C and 3). Its increased expression is commonly associated with oxidative stress, where it either reflects or promotes redox imbalance. Thus, CHAC1 upregulation in our system is consistent with activation of oxidative stress and supports a model in which chronic exposure induces redox disruption. Therefore, upregulation of CHAC1 can contribute to the glutathione depletion, promoting susceptibility to cell death.

It is important to note that, in addition to CHAC1, we observed upregulation of activating transcription factor 3 (ATF3), a transcription factor that is acutely induced under oxidative and cellular stress conditions (Fig. 2C).[50,51] Both CHAC1 and ATF3 are downstream targets of the integrated

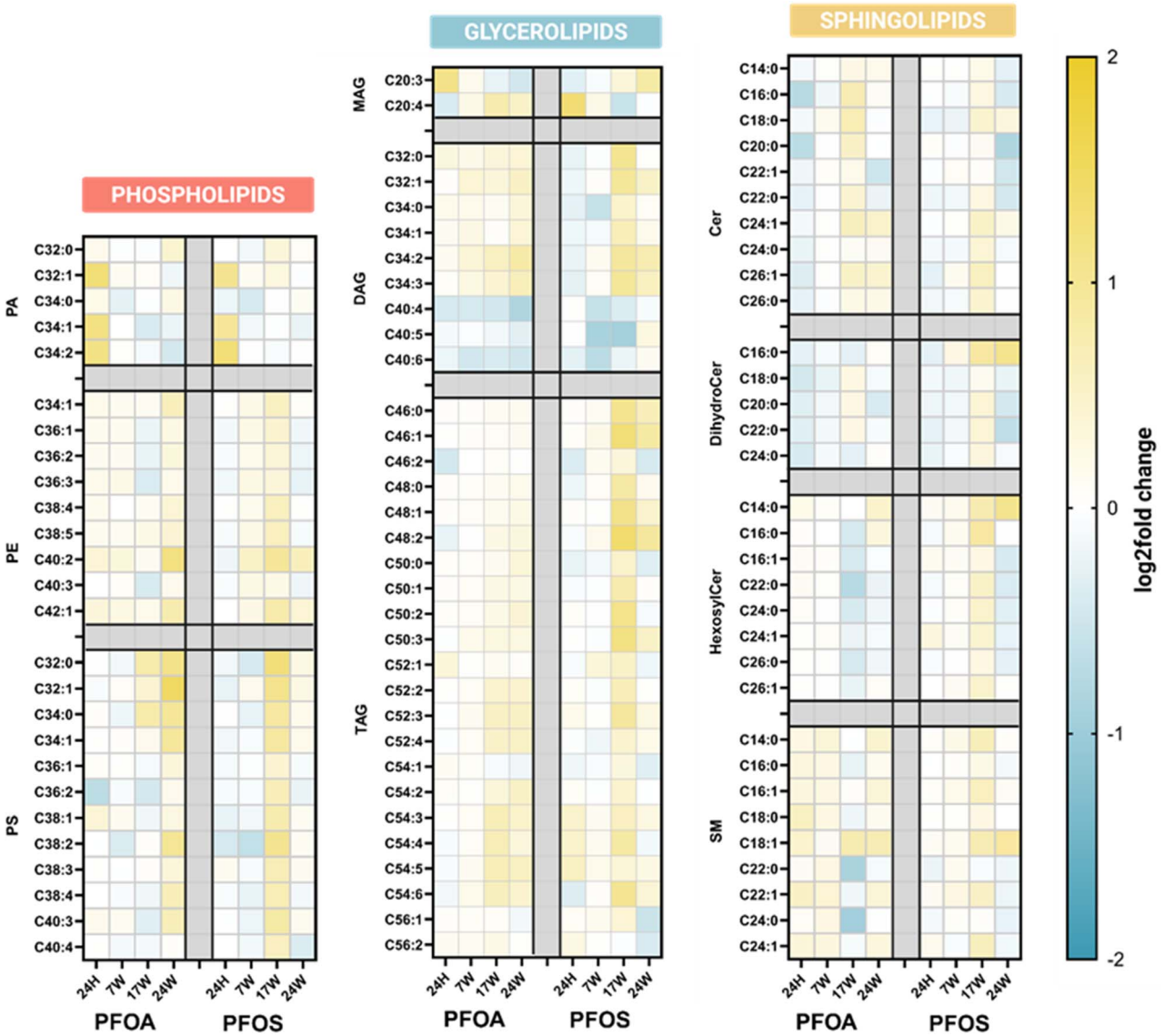


Fig. 4 Heatmap representation of lipidomic alterations in hTERT RPE-1 cells following prolonged PFOA and PFOS exposure. The profiles reveal changes across major lipid classes, including phospholipids [phosphatidic acid (PA), phosphatidylethanolamine (PE), and phosphatidylserine (PS)], glycerolipids [monoacylglycerol (MAG), diacylglycerol (DAG), and triacylglycerol (TAG)], and sphingolipids [ceramide (Cer), dihydroceramide (DihydroCer), hexosylceramide (HexosylCer), and sphingomyelin (SM)] in PFOA- and PFOS-treated cells. The $\log_2$fold changes were calculated by dividing individual abundances by the average of each corresponding time point vehicle (MeOH) control. The $\log_2$ of this ratio was taken and averaged across three replicates (refer to Table S3 for individual values).

stress response pathway and are commonly upregulated in response to ROS accumulation and glutathione depletion.[52] The coordinated induction of these genes suggests activation of a redox-sensitive transcriptional program.[48]

Altogether, gene expressions in Fig. 3 peak at 24 weeks for both PFOA and PFOS treatments, indicating a shared oxidative stress response pattern. Taken together, these findings suggest that cellular stress, lipid metabolism, and cell death pathways are modulated during PFAS exposure as part of an integrated cellular response to oxidative stress. Our findings align with a recent study[53] indicating that PFAS can induce oxidative stress and DNA damage in human liver cells, with PFOA being particularly significant.

### 3.5. PFAS exposure rewires the cellular lipidome in a time- and compound-specific manner

Studies have shown that both PFOA and PFOS can induce changes in lipid homeostasis *in vitro*,[54,55] albeit primarily under high concentrations and short-term treatments. Further, transcriptomic data indicate that several lipid metabolism-related genes are differentially expressed. These observations prompted us to investigate whether these transcriptional changes translate into alterations in the cellular lipidome. We performed lipidomic profiling following prolonged exposure to PFOA and PFOS. Similar to our transcriptomics experimental design, we treated cells with PFOA or PFOS for 24 hours, 7 weeks, 17 weeks, and 24 weeks, and collected them for

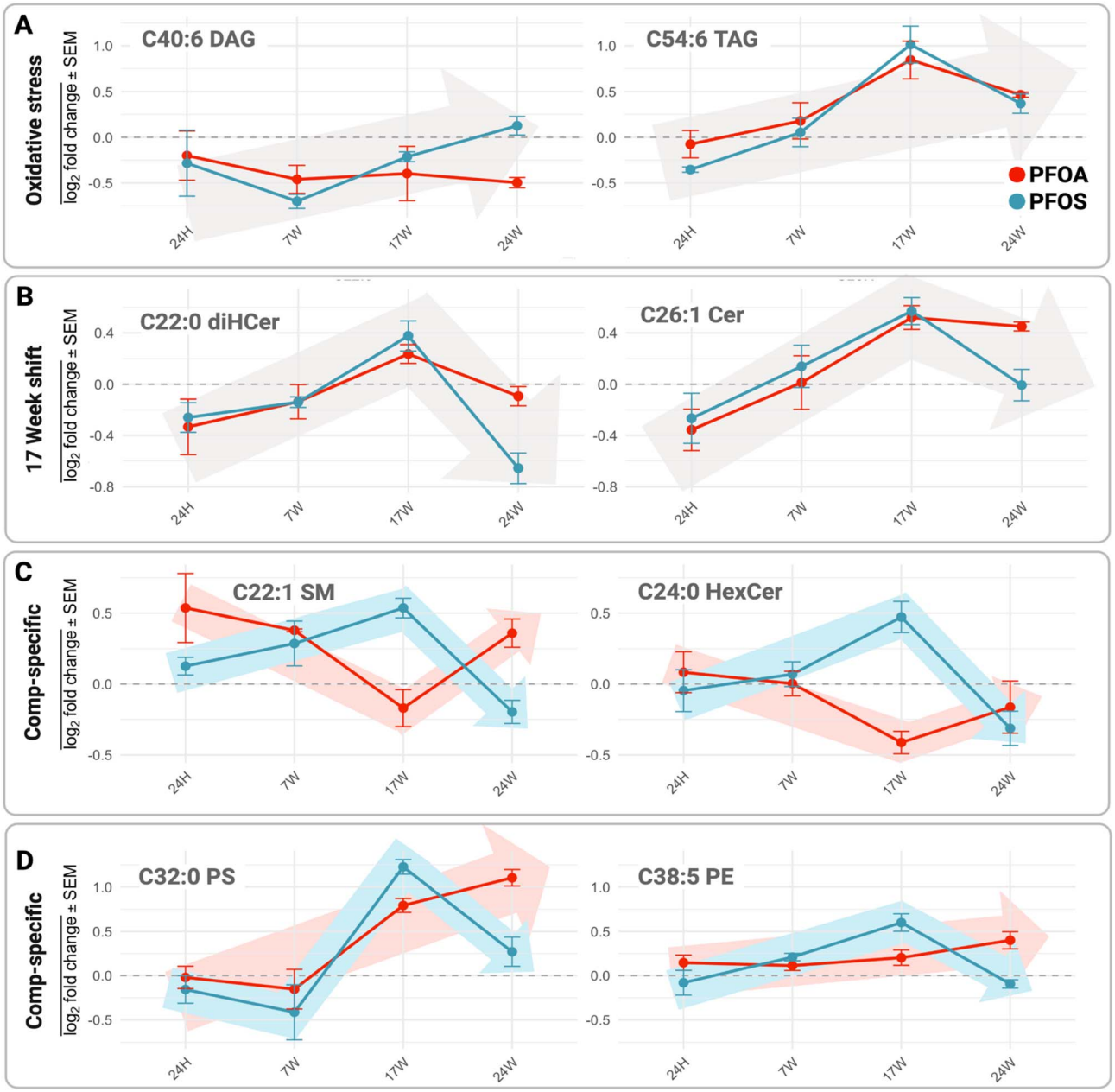


Fig. 5 Representative time plots of changes in lipid levels over time following PFOA and PFOS exposure. (A) Levels of representative long unsaturated diacylglycerols (DAGs) (C40:6) as precursors for triacylglycerol (TAG) biosynthesis, and polyunsaturated TAGs (C54:6) are shown. (B) A representative peaking of lipid levels at 17 weeks for both PFOA and PFOS in dihydroxyceramides (diHCer) (C22:0), and ceramides (Cer) (C26:1). (C) Opposite trend on lipid levels observed in PFOA and PFOS in sphingomyelin (SM) (C22:1) and in hexosylceramide (HexCer) (C24:0), (D) compound-specific trend observed in phosphatidylserine (PS) (C32:0), and phosphatidylethanolamine (PE) (C38:5), where PFOA shows upregulation until 24 weeks while PFOS peaks at 17 weeks. Data are presented as $\log_2$fold change ± SEM from three independent replicates.

lipidomics analysis. Because lipid changes over time in this cell line have not been previously characterized, we obtained vehicle controls for each corresponding time point. Consequently, our comparative lipidomics analysis focused on evaluating the lipid composition of PFOA- and PFOS-treated samples relative to their matched vehicle (MeOH) controls.

We targeted members from major mammalian lipid classes (Fig. 4, S3 and Table S3). We found that both PFOA and PFOS reshape the cellular lipidome over time. This finding is consistent with a recent study showing that PFAS exposure alters lipid metabolism and cholesterol regulation in human liver microtissues and differentiated neuroblastoma cells.[56] Among the lipid alterations observed, phosphatidic acid species exhibited a transient increase in both PFOA- and PFOS-treated cells at the 24 hour time point, followed by a return to baseline levels at later exposure durations (Fig. 4). Phosphatidic acid is a central intermediate in membrane lipid metabolism and a known target of lipid peroxidation under oxidative stress. Its

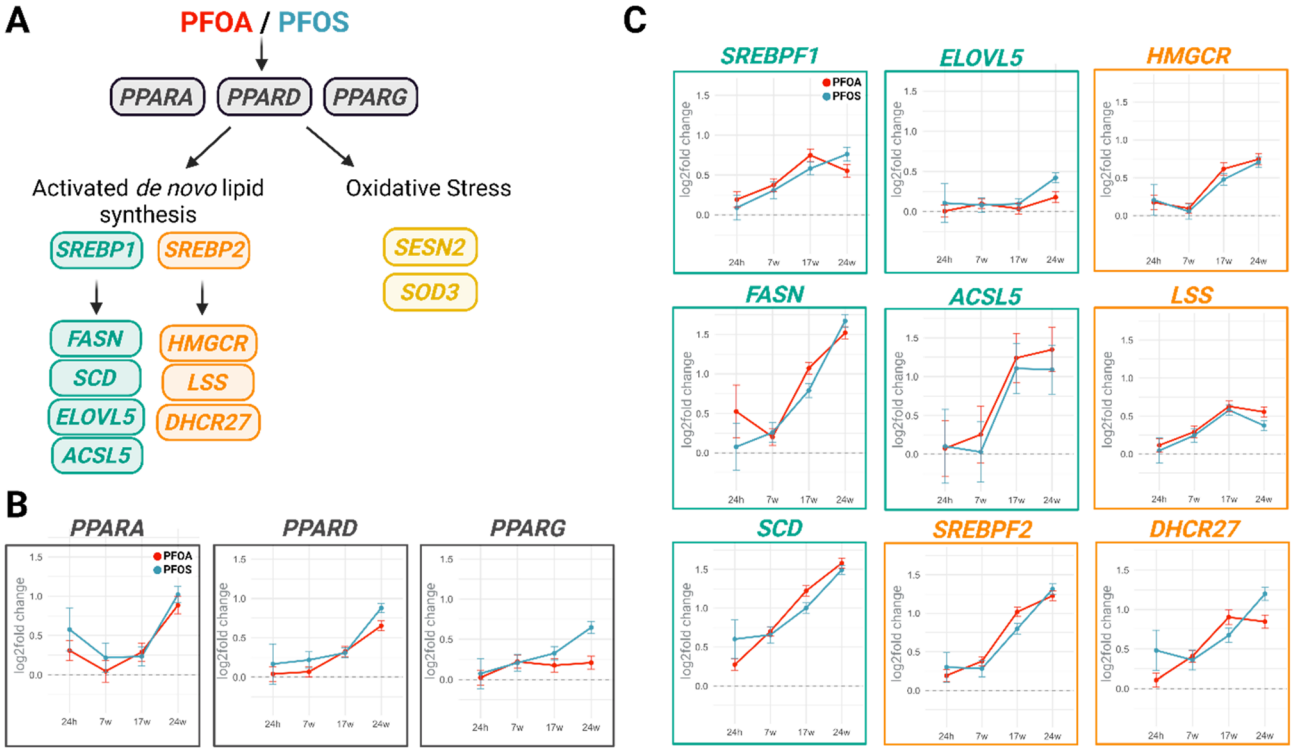


Fig. 6 PFOA and PFOS exposure activate PPARs and SREBPs, upregulating key genes in *de novo* lipid biosynthesis. (A) Lipid biosynthesis pathways impacted by prolonged PFOA and PFOS exposure lead to oxidative stress, with upregulated Sestrin 2 (SESN2), Superoxide dismutase 3 (SOD3), and activated *de novo* lipid synthesis. (B) These pathways involve peroxisome proliferator-activated receptors (PPARs) such as PPARA, PPARD, and PPARG. (C) The activation of these PPARs leads to transcriptional regulation of genes involved in *de novo* lipid synthesis through Sterol Regulatory Element Binding Protein-1 (SREBP1) [Fatty acid synthase (FASN), Stearoyl-CoA desaturase (SCD), Elongation of very long chain fatty acid 5 (ELOVL5), Acyl-CoA synthetase long chain family member 5 (ACSL5)], and Sterol Regulatory Element Binding Protein-2 (SREBP2) [3-hydroxy-3-methyl-glutaryl-coenzyme A reductase (HMGCR), Lanosterol synthase (LSS), and 7-dehydrocholesterol reductase (DHCR27)]. Data are presented as $\log_2$fold change ± SEM from three independent replicates.

accumulation has been associated with membrane destabilization and increased susceptibility to oxidative damage.[57] Thus, the observed changes in phosphatidic acid levels can indicate a mechanism to mitigate oxidative stress.

In parallel, we observed persistently low levels of long-chain unsaturated diacylglycerols, which serve as precursors for triacylglycerol synthesis (Fig. 4). Notably, this decrease was most pronounced for polyunsaturated diacylglycerol species. This trend may reflect another protective cellular strategy, as supported by a previous study.[58] Specifically, the upregulation of Diacylglycerol O-Acyltransferase 1 (DGAT1) (Table S5), which catalyzes triacylglycerol synthesis, could indicate a mechanism to sequester polyunsaturated fatty acid-containing lipids away from membranes. Consistent with this interpretation, diversion of polyunsaturated acyl chains into triacylglycerols has been reported as an adaptive response to oxidative stress. Such sequestration is known to reduce oxidative damage[59] during cell death by preventing lipid peroxidation of unsaturated fatty acyl chains. Taken together, our results suggest that PFOA and PFOS induce a chronic lipotoxic environment characterized by early and persistent neutral lipid storage and reduction in phosphatidic acids. In this context, the reduction in polyunsaturated diacylglycerols and increased neutral lipid storage is consistent with a stress-driven redistribution of lipids. This stress-driven remodeling helps explain deviations from the otherwise general trend of increased lipid biosynthesis in PFAS-exposed cells and underscores the complexity of the cellular lipid response under chronic chemical stress.

### 3.6. Lipid remodeling evident by 17 weeks highlights distinct effects of PFOA and PFOS

In contrast to the relatively linear patterns observed in gene expression, lipid abundance followed complex, compound-specific trajectories (Fig. 4). Rather than a consistent accumulation or depletion across the lipid family, many lipid species showed dynamic, time-dependent changes, with the 17 week time point emerging as a divergent point among the sampled time points.

One of the most notable and unexpected trends we observed was the initial accumulation of multiple lipid species, which peaked at 17 weeks and declined at 24 weeks (Fig. 4 and Table S3). For example, PFOA exposure led to a sustained buildup of glycerolipids, particularly triacylglycerols, from early exposure through 24 weeks (Fig. 4). This pattern suggests a diversion of fatty acids into storage lipid droplets that persists for PFOA expression. In contrast, the triacylglycerol levels, such as C54:6 TAG, in PFOS-treated samples declined after 17 weeks,

returning to or dropping below baseline levels by 24 weeks (Fig. 4, 5A and Table S3).

A comparable temporal pattern was also observed for ceramides and dihydroceramides, such as C26:1 Cer and C22:0 diHCer, which were elevated at 17 weeks in both PFOA- and PFOS-treated cells but declined by 24 weeks (Fig. 4 and 5B). These compound-specific, time-dependent differences may arise from distinct membrane interactions driven by differing headgroup chemistry, carboxylate (PFOA) *versus* sulfonate (PFOS), which influence membrane penetration, orientation, and affinity. Supporting this, PFOS exposure increased levels of representative sphingomyelin (C22:1 SM) and hexosylceramide (C24:0 HexCer), peaking at 17 weeks and then normalizing by 24 weeks, whereas PFOA exposure markedly reduced both lipids at 17 weeks and normalized them by 24 weeks (Fig. 4 and 5C).

Phosphatidylserines (*e.g.* C32 PS) and phosphatidylethanolamines (*e.g.* C38:5 PE) also exhibited a distinct temporal pattern. PFOA exposure resulted in a gradual increase in these lipid species, reaching peak levels at 24 weeks. In contrast, PFOS exposure induced more dynamic fluctuations, with levels peaking at 17 weeks before declining (Fig. 4 and 5D). This suggests PFAS interact with cellular membranes, and the timing of cellular responses influences long-term exposure. The exposure-specific, time-dependent differences observed in lipid species may arise from distinct interactions between PFOA or PFOS cellular membranes. Further studies are warranted to identify the mechanisms that result in these distinct regulations and their consequences for PFAS exposure.

### 3.7. PFAS exposure leads to a general increase in lipid biosynthesis

Previous studies have suggested that PFAS can interact with membranes and interfere with membrane structure and function, triggering compensatory responses through lipid biosynthesis pathways.[60,61] One mechanism involves the activation of peroxisome proliferator-activated receptors (PPARs), which regulate transcriptional programs that promote lipid synthesis (Fig. 6A).[61] Consistent with this, we observed upregulation of multiple PPARs (Fig. 6B) and key lipid biosynthesis regulators downstream of PPAR signaling, including Sterol Regulatory Element Binding Transcription Factor-1 (SREBF1) and Sterol Regulatory Element Binding Transcription Factor-2 (SREBF2).

The upregulation of SREBF1 and SREBF2 is critical in lipid biosynthesis pathways. These genes encode the precursors of the transcription factors SREBP1 and SREBP2, which are master regulators of de novo fatty acid, phospholipid, and sterol biosynthesis (Fig. 6A, C and Table S5).[62] Their function depends on spatial translocation from the endoplasmic reticulum membrane to the Golgi apparatus,[63] where they undergo proteolytic cleavage to generate their active DNA-binding forms. These active forms then translocate to the nucleus to initiate lipid synthesis gene expression. Further, we found a concurrent upregulation of SREBP Cleavage-Activating Protein (SCAP), which encodes an adaptor protein essential for activation of these two SREBPs, further corroborating the involvement of SREBPs in PFOA- and PFOS-mediated lipid modeling.[63]

Activation of SREBP downstream targets could result in complex alterations in lipid species, including those involved in glycerolipid and phospholipid synthesis that we observed upon PFOA and PFOS exposure (Fig. 6A). Consistent with this idea, PFAS exposure leads to increased expression of the downstream targets of SREBP1 (Fig. 6C). These targets include key enzymes involved in fatty acid synthesis (FASN), activation (ACSL5), elongation (ELOVL5), and desaturation (SCD). The expression shifts in these enzymes could underlie the observed increases in glycerolipid and phospholipid species in our lipidomic data. Similarly, SREBP2 target genes were also upregulated, including those encoding enzymes required for sterol biosynthesis (Fig. 6C). Notably, HMGCR, which encodes HMG-CoA reductase, the rate-limiting enzyme in sterol synthesis,[64] was upregulated alongside downstream enzymes involved in sterol formation, such as lanosterol synthase (LSS).[65] Together, these findings suggest a coordinated increase in lipid production through de novo synthesis pathways, regulated by the SREBP signaling axis, in response to chronic PFOA and PFOS exposure.

## 4. Conclusions

This study centers on defining time-resolved molecular and lipidomic responses to chronic PFOA and PFOS exposure and provides a framework for future functional investigations. Altogether, our study reveals that prolonged exposure to environmentally relevant concentrations of PFOA and PFOS elicits robust, time-dependent cellular responses in the absence of significant intracellular PFAS accumulation. These findings suggest that chronic PFAS toxicity may not require sustained intracellular buildup but instead may arise from persistent cellular interactions, including perturbation of membrane biophysical properties. Importantly, we show a divergence in lipid profiles between PFOA- and PFOS-treated cells, particularly among sphingolipids and membrane phospholipids. These compound-specific trends support a model in which subtle differences in PFAS headgroup properties can lead to distinct biophysical membrane interactions and different cellular outcomes over time.

Overall, these findings suggest a multilayered, systems-level response involving oxidative stress, transcriptional regulation of lipid metabolism, and membrane remodeling following chronic PFAS exposure. The use of hTERT RPE-1 cells enabled long-term exposure under stable, non-transformed conditions, allowing resolution of delayed molecular responses that are difficult to capture in short-term or cancer-derived models. At the same time, we acknowledge that this single-cell-type i*n vitro* system cannot fully recapitulate the complexity of PFAS toxicokinetics or tissue-specific responses observed *in vivo*, particularly in organs with high PFAS burden or specialized barrier functions. Nevertheless, the molecular signatures identified here provide a framework for understanding how low-dose PFAS exposure can drive cellular stress responses independent of overt accumulation. While the transcriptomic and lipidomic signatures identified here may suggest associations with oxidative stress, membrane remodeling, and adaptive cellular responses, future studies that integrate additional cell

types, functional phenotypic assays, and *in vivo* models will be essential to elucidate how membrane-associated PFAS interactions and adaptive lipid remodeling contribute to long-term health outcomes.

## Author contributions

The manuscript was written through the contributions of all authors. Conceptualization: JZP, JRC, OG, DSA, GEAG, investigation: JZP, JRC, LJBL, ALG, visualization: JZP, JRC, LJBL, supervision: OG, DSA, GEAG, writing – original draft: JZP, JRC, OG, DSA, GEAG, writing – review & editing: JZP, JRC, LJBL, OG, DSA, GEAG. All authors have approved the final version of the manuscript.

## Conflicts of interest

There are no conflicts to declare.

## Data availability

Data are available in the main text. The RNA-seq raw sequencing data (FASTQ files) generated in this study have been deposited in the NCBI BioProject database under accession number PRJNA1425030 and in the NCBI Gene Expression Omnibus (GEO) under accession number GSE320486. All data supporting the findings of this study are available within supplementary information (SI). Supplementary information: including analytical method parameters and performance metrics, lipidomics and uptake datasets, transcriptomic differential expression and gene ontology analyses, and associated figures. See DOI: https://doi.org/10.1039/d5va00353a.

## Acknowledgements

The authors would like to acknowledge UB RENEW Institute for the use of analytical instrumentation and staff support. This work was supported by the SUNY Research Foundation SEED Grant 241056 (DSA) and National Institute of Environmental Health Sciences grant R01ES036199 (GEAG). The opinions, findings, conclusions, or recommendations presented in this publication are solely those of the author(s) and do not necessarily represent the views of the funding agencies.

## References

1 M. B. Ahmed, M. A. H. Johir, R. McLaughlan, L. N. Nguyen, B. Xu and L. D. Nghiem, *Sci. Total Environ.*, 2020, **748**, 141251, DOI: 10.1016/j.scitotenv.2020.141251.
2 G. R. Johnson, M. L. Brusseau, K. C. Carroll, G. R. Tick and C. M. Duncan, *Sci. Total Environ.*, 2022, **841**, 156602, DOI: 10.1016/j.scitotenv.2022.156602.
3 M. Antonopoulou, A. Spyrou, A. Tzamaria, I. Efthimiou and V. Triantafyllidis, *Sci. Total Environ.*, 2024, **913**, 169332, DOI: 10.1016/j.scitotenv.2023.169332.
4 S. Y. Wee, A. Z. Aris, S. Y. Wee and A. Z. Aris, *npj Clean Water*, 2023, **6**, 57, DOI: 10.1038/s41545-023-00274-6.
5 W. Olsen, J. M. Burris, D. J. Ehresman, J. W. Froehlich, A. M. Seacat, J. L. Butenhoff and L. R. Zobel, *Environ. Health Perspect.*, 2007, **115**(9), 1298–1305, DOI: 10.1289/ehp.10009.
6 L. Gaillard, R. Barouki, E. Blanc, X. Coumoul and K. Andréau, *Trends Endocrinol. Metab.*, 2025, **36**(3), 249–261, DOI: 10.1016/j.tem.2024.07.021.
7 P. Deng, J. Durham, J. Liu, X. Zhang, C. Wang, D. Li, T. Gwag, M. Ma and B. Hennig, *Environ. Health Perspect.*, 2022, **130**(11), 117003, DOI: 10.1289/EHP11360.
8 B. Pachkowski, G. B. Post and A. H. Stern, *Environ. Res.*, 2019, **171**, 452–469, DOI: 10.1016/j.envres.2018.08.004.
9 S. E. Fenton, A. Ducatman, A. Boobis, J. C. DeWitt, C. Lau, C. Ng, J. S. Smith and S. M. Roberts, *Environ. Toxicol. Chem.*, 2020, **40**(3), 606–630, DOI: 10.1002/etc.4890.
10 L. Running, J. R. Cristobal, C. Karageorgiou, M. Camdzic, J. M. N. Aguilar, O. Gockumen, D. S. Aga and G. E. Atilla-Gokcumen, *ACS Chem. Neurosci.*, 2024, **15**(24), 4568–4579, DOI: 10.1021/acschemneuro.4c00652.
11 J. A. Goodrich, D. Walker, X. Lin, H. Wang, T. Lim, R. McConnell, D. V. Conti, L. Chatzi and V. W. Setiawan, Exposure to perfluoroalkyl substances and risk of hepatocellular carcinoma in a multiethnic cohort, *JHEP Rep.*, 2022, **4**, 10050, DOI: 10.1016/j.jhepr.2022.100550.
12 K. M. Ríos-Bonilla, D. S. Aga, J. Lee, M. König, W. Qin, J. R. Cristobal, G. E. Atilla-Gokcumen and B. I. Escher, *Environ. Sci. Technol.*, 2024, **58**, 16774–16784, DOI: 10.1021/acs.est.4c06017.
13 M. Camdzic, D. S. Aga and G. E. Atilla-Gokcumen, *Chem. Res. Toxicol.*, 2022, **35**(4), 694–702, DOI: 10.1021/acs.chemrestox.2c00078.
14 A. Naumann, J. Alesio, M. Poonia and G. D. Bothun, *J. Environ. Chem. Eng.*, 2022, **10**, 107351, DOI: 10.1016/j.jece.2022.107351.
15 L. Zhao, M. Teng, X. Zhao, Y. Li, J. Sun, W. Zhao, Y. Ruan, K. M. Y. Leung and F. Wu, *Environ. Int.*, 2023, **175**, 107951, DOI: 10.1016/j.envint.2023.107951.
16 N. M. S. Almeida, S. K. Bali, D. James, C. Wang and A. K. Wilson, *J. Chem. Inf. Model.*, 2023, **63**, 7423–7443, DOI: 10.1021/acs.jcim.3c01384.
17 D. S. Garcia, M. Sjödin, M. Hellstrandh, U. Norinder, V. Nikiforova, J. Lindberg, E. Wincent, Å. Bergman, I. Cotgreave and V. M. Kos, *Chem.-Biol. Interact.*, 2018, **281**, 1–10, DOI: 10.1016/j.cbi.2017.12.021.
18 S. Zheng, P. Sarker, D. Gursoy, T. Wei and B. S. Hsiao, *Langmuir*, 2025, **41**, 9369–9376, DOI: 10.1021/acs.langmuir.5c00124.
19 F. C. Fischer, S. Ludtke, C. Thackray, H. M. Pickard, F. Haque, C. Dassuncao, S. Endo, L. Schaider and E. M. Sunderland, *Environ. Sci. Technol.*, 2024, **58**(2), 1055–1063, DOI: 10.1021/acs.est.3c07415.
20 L. Zhang, X.-M. Ren and L.-H. Guo, *Environ. Sci. Technol.*, 2013, **47**(19), 11293–11301, DOI: 10.1021/es4026722.
21 T. A. Slotkin, E. A. MacKillop, R. L. Melnick, K. A. Thayer and F. J. Seidler, Developmental Neurotoxicity of Perfluorinated Chemicals Modeled in Vitro, *Environ. Health Perspect.*, 2008, **116**(6), 716–722, DOI: 10.1289/ehp.11253.

22 C. H. Lindh, L. Rylander, G. Toft, A. Axmon, A. Rignell-Hydbom, A. Giwercman, H. S. Pedersen, K. Góalczyk, J. K. Ludwicki, V. Zvyezday, R. Vermeulen, V. Lenters, D. Heederik, J. P. Bonde and B. A. G. Jönsson, *Chemosphere*, 2012, **88**, 1269–1275, DOI: 10.1016/j.chemosphere.2012.03.049.

23 J. Pan, C. Ouyang, S. Zhou, X. Wang, H. Liu, J. Zhang, X. Wang, X. Shi, A. Yang and X. Hu, *Toxics*, 2024, **12**, 314, DOI: 10.3390/toxics12050314.

24 E. Volpe, A. Colantoni, L. Corda, E. Di Tommaso, F. Pelliccia, R. Ottalevi, A. Guarracino, D. Licastro, L. Faino, M. Capulli, G. Formenti, E. Tassone, S. Giunta, E. Volpe, A. Colantoni, L. Corda, E. Di Tommaso, F. Pelliccia, R. Ottalevi, A. Guarracino, D. Licastro, L. Faino, M. Capulli, G. Formenti, E. Tassone and S. Giunta, *Nat. Commun.*, 2025, **16**, 7751, DOI: 10.1038/s41467-025-62428-z.

25 J. J. Miciak, L. Petrova, R. Sajwan, A. Pandya, M. Deckard, A. J. Munoz, F. Bunz, J. J. Miciak, L. Petrova, R. Sajwan, A. Pandya, M. Deckard, A. J. Munoz and F. Bunz, *Oncotarget*, 2025, **16**, 79–100, DOI: 10.18632/oncotarget.28690.

26 D. Camdzic, H. K. Welgama, M. R. Crawley, A. Avasthi, T. R. Cook and D. S. Aga, *ACS Appl. Eng. Mater.*, 2024, **2**, 87–95, DOI: 10.1021/acsaenm.3c00592.

27 M. I. Love, W. Huber, S. Anders, M. I. Love, W. Huber and S. Anders, *Genome Biol.*, 2014, **15**, 550, DOI: 10.1186/s13059-014-0550-8.

28 L. Kolberg, U. Raudvere, I. Kuzmin, P. Adler, J. Vilo and H. Peterson, *Nucleic Acids Res.*, 2023, **51**, W207–W212, DOI: 10.1093/nar/gkad347.

29 N. Li, D. Y. Lizardo and G. E. Atilla-Gokcumen, *ACS Chem. Biol.*, 2016, **11**(9), 2583–2587, DOI: 10.1021/acschembio.6b00410.

30 M. Camdzic, D. S. Aga and G. E. Atilla-Gockumen, *Environ. Health*, 2023, **1**(2), 2583–2587, DOI: 10.1021/envhealth.3c00022.

31 N. L. Hindul, A. Jhita, D. G. Oprea, T. A. Hussain, O. Gonchar, M. A. M. Campillo, L. O'Regan, M. T. Kanemaki, A. M. Fry, K. Hirota and K. Tanaka, *Biol. Open*, 2022, **11**(2), bio059056, DOI: 10.1242/bio.059056.

32 *A Review of the Reference Dose and Reference Concentration Processes*, https://www.epa.gov/osa/review-reference-dose-and-reference-concentration-processes, accessed October 8, 2025.

33 I. Rosato, T. Bonato, T. Fletcher, E. Batzella and C. Canova, *Environ. Res.*, 2024, **242**, 117743, DOI: 10.1016/j.envres.2023.117743.

34 Y. Zhang, S. Beesoon, L. Zhu and J. W. Martin, *Environ. Sci. Technol.*, 2013, **47**, 10619–10627, DOI: 10.1021/es401905.

35 M. Xu, J. Wan, Q. Niu and R. Liu, *Environ. Res.*, 2019, **175**, 63–70, DOI: 10.1016/j.envres.2019.05.008.

36 X. Li, K. Jing, L. He, P. Song and J. Yu, *Toxicology*, 2025, **517**, 154218, DOI: 10.1016/j.tox.2025.154218.

37 A. Koeberle, K. Löser and M. Thürmer, *Biochim. Biophys. Acta, Mol. Cell Biol. Lipids*, 2016, **1861**(11), 1719–1726, DOI: 10.1016/j.bbalip.2016.08.009.

38 S.-H. Ro, M. Nam, I. Jang, H.-W. Park, H. Park, I. A. Semple, M. Kim, J. S. Kim, H. Park, P. Einat, G. Damari, M. Golikov, E. Feinstein and J. H. Lee, *Proc. Natl. Acad. Sci. U. S. A.*, 2014, **111**, 7849–7854, DOI: 10.1073/pnas.1401787111.

39 H. Matsui, T. Yokoyama, K. Sekiguchi, D. Iijima, H. Sunaga, M. Maniwa, M. Ueno, T. Iso, M. Arai and M. Kurabayashi, *J. Mol. Cell. Cardiol.*, 2012, **52**, 719–728, DOI: 10.1371/journal.pone.0033283.

40 Z. Liu, L. Zhao, T. Gao, C. Li and Y. Sun, *Biochem. Biophys. Res. Commun.*, 2025, **789**, 152849, DOI: 10.1016/j.bbrc.2025.152849.

41 E. D. F. Zachariae, L. Hu and S. V. Petersen, *Oxidative Stress*, 2020, DOI: 10.1016/B978-0-12-818606-0.00012-2.

42 A. Haidurov and A. V. Budanov, *Mech. Ageing Dev.*, 2020, **192**, 111379, DOI: 10.1016/j.mad.2020.111379.

43 S. Cavallero, M. Roustaei, S. Satta, J. M. Cho, H. Phan, K. I. Baek, A. M. Blázquez-Medela, S. Gonzalez-Ramos, K. Vu, S.-K. Park, T. Yokota, J. Sumner, J. J. Mack, C. D. Sigmund, S. T. Reddy, R. Li and T. K. Hsiai, *Sci. Adv.*, 2024, **10**, eadj7481, DOI: 10.1126/sciadv.adj7481.

44 C. M. Paton and J. M. Ntambi, *Am. J. Physiol.: Endocrinol. Metab.*, 2009, **297**(1), E28–E37, DOI: 10.1152/ajpendo.90897.2008.

45 W. S. Yang, K. J. Kim, M. M. Gaschler, M. Patel, M. S. Shchepinov and B. R. Stockwell, *Proc. Natl. Acad. Sci. U. S. A.*, 2016, **113**(34), 4966–4975, DOI: 10.1073/pnas.1603244113.

46 Q. Luo, A. Das, F. Oldoni, P. Wu, J. Wang, F. Luo and Z. Fang, *Heliyon*, 2023, **9**, el3316, DOI: 10.1016/j.heliyon.2023.e13316.

47 E. L. Seifert, C. Estey, J. Y. Xuan and M.-E. Harper, *J. Biol. Chem.*, 2010, **285**(8), 5748–5758, DOI: 10.1074/jbc.M109.026203.

48 L. P. Kolligundla, K. M. Sullivan, D. Mukhi, M. Andrade-Silva, H. Liu, Y. Guan, X. Gu, J. Wu, T. Doke, D. Hirohama, P. Guarnieri, J. Hill, S. S. Pullen, J. Kuo, M. Inamoto and K. Susztak, *Sci. Transl. Med.*, 2025, **17**, eadn3079, DOI: 10.1126/scitranslmed.adn3079.

49 A. Kumar, S. Tikoo, S. Maity, S. Sengupta, S. Sengupta, A. Kaur and A. K. Bachhawat, *EMBO Rep.*, 2012, **13**(12), 1095–1101, DOI: 10.1038/embor.2012.156.

50 T. Nyunt, M. Britton, K. Wanichthanarak, M. Budamagunta, J. C. Voss, D. W. Wilson, J. C. Rutledge and H. H. Aung, *Free Radical Biol. Med.*, 2019, **143**, 25–46, DOI: 10.1016/j.freeradbiomed.2019.07.024.

51 M. Rohini, A. H. Menon and N. Selvamurugan, *Int. J. Biol. Macromol.*, 2018, **120**, 310–317, DOI: 10.1016/j.ijbiomac.2018.08.107.

52 W. Hoetzenecker, B. Echtenacher, E. Guenova, K. Hoetzenecker, F. Woelbing, J. Brück, A. Teske, N. Valtcheva, K. Fuchs, M. Kneilling, J.-H. Park, K.-H. Kim, K.-W. Kim, P. Hoffmann, C. Krenn, T. Hai, K. Ghoreschi, T. Biedermann and M. Röcken, *Nat. Med.*, 2011, **18**, 128–134, DOI: 10.1038/nm.2557.

53 M. Wielsøe, M. Long, M. Ghisari and E. C. Bonefeld-Jørgensen, *Chemosphere*, 2015, 129, DOI: 10.1016/j.chemosphere.2014.10.014.

54 X. Gou, M. Tian, L. Yan, P. Xia, H. Ji, H. Tan, W. Shi, H. Yu and X. Zhang, *Environ. Int.*, 2024, **191**, 108962, DOI: 10.1016/j.envint.2024.10896.
55 J. Louisse, D. Rijkers, G. Stoopen, A. Janssen, M. Staats, R. Hoogenboom, S. Kersten, A. Peijnenburg, J. Louisse, D. Rijkers, G. Stoopen, A. Janssen, M. Staats, R. Hoogenboom, S. Kersten and A. Peijnenburg, *Arch. Toxicol.*, 2020, **94**, 3137–3155, DOI: 10.1007/s00204-020-02808-0.
56 G. C. Addicks, A. Rowan-Carroll, K. Leingartner, A. Williams, M. J. Meier, L. Lorusso, C. L. Yauk and E. Atlas, *Toxicol. Sci.*, 2025, **207**, 161–180, DOI: 10.1093/toxsci/kfaf075.
57 I. L. Yurkova, F. Stuckert, M. A. Kisel, O. I. Shadyro, J. Arnhold and D. Huster, *Arch. Biochem. Biophys.*, 2008, **480**, 17–26, DOI: 10.1016/j.abb.2008.09.007.
58 N. Li, Y. Sancak, J. Frasor and G. E. Atilla-Gokcumen, *Biochemistry*, 2017, **57**, 72–80, DOI: 10.1021/acs.biochem.7b00975.
59 A. P. Bailey, G. Koster, C. Guillermier, E. M. A. Hirst, J. I. MacRae, C. P. Lechene, A. D. Postle and A. P. Gould, *Cell*, 2015, **163**(2), 340–353, DOI: 10.1016/j.cell.2015.09.020.
60 F. Sadrabadi, J. Alarcan, H. Sprenger, A. Braeuning, T. Buhrke, F. Sadrabadi, J. Alarcan, H. Sprenger, A. Braeuning and T. Buhrke, *Arch. Toxicol.*, 2023, **98**(2), 507–524, DOI: 10.1007/s00204-023-03649-3.
61 S. Fragki, H. Dirven, T. Fletcher, B. Grasl-Kraupp, K. B. Gützkow, R. Hoogenboom, S. Kersten, B. Lindeman, J. Louisse, A. Peijnenburg, A. H. Piersma, H. M. G. Princen, M. Uhl, J. Westerhout, M. J. Zeilmaker and M. Luijten, *Crit. Rev. Toxicol.*, 2021, **51**(2), 141–164, DOI: 10.1080/10408444.2021.1888073.
62 R. Bertolio, F. Napoletano, M. Mano, S. Maurer-Stroh, M. Fantuz, A. Zannini, S. Bicciato, G. Sorrentino, G. Del Sal, R. Bertolio, F. Napoletano, M. Mano, S. Maurer-Stroh, M. Fantuz, A. Zannini, S. Bicciato, G. Sorrentino and G. Del Sal, *Nat. Commun.*, 2019, **1038**, 1326, DOI: 10.1038/s41467-019-09152-7.
63 W. Shao and P. J. Espenshade, *J. Biol. Chem.*, 2014, **289**, 7547–7557, DOI: 10.1074/jbc.M113.545699.
64 L. Chen, M.-Y. Ma, M. Sun, L.-Y. Jiang, X.-T. Zhao, X.-X. Fang, S. M. Lam, G.-H. Shui, J. Luo, X.-J. Shi and B.-L. Song, *J. Lipid Res.*, 2019, **60**(10), 1765–1775, DOI: 10.1194/jlr.M093518.
65 A. J. Brown and L. J. Sharpe, *Biochemistry of Lipids, Lipoproteins and Membranes*, 2016, DOI: 10.1016/B978-0-444-63438-2.00011-0.